Electronic and carrier transport properties of small molecule donors

Ramon Valencia-Maturana and Chun-Wei Pao[*]

Research Center for Applied Sciences, Academia Sinica, Taipei 11529, Taiwan

Abstract.   As electron donor/acceptor materials for organic photovoltaic cells, small-molecules donors/acceptor are attracting more and more attention. In this work, we investigated the electronic structures, electrochemical properties, and charge carrier transport properties of four recently-synthesized small-molecule donors/acceptor, namely, DPDCPB (A), DPDCTB (B), DTDCPB (A1), and DTDCTB (B1), by a series of *ab initio* calculations. The calculations look into the electronic structure of singly oxidized and reduced molecules, the first anodic and cathodic potentials, and the electrochemical gaps. Results of our calculations were in accord with those from experiments. Using Marcus theory, we also computed the reorganization energies of hole/electron hoppings, as well as hole/electron transfer integrals of multiple possible molecular dimer configurations. Our calculations indicated that the electron/hole transport properties are very sensitive to the relative separations/orientations between neighboring molecules. Due to high reorganization energies for electron hopping, the hole mobilities in the molecular crystals are at least an order of magnitude higher than the electron mobilities.

Keywords: electronic structure; charge carrier transport; morphology; small molecule organic solar cell

1. Introduction

The conversion of solar energy into electricity is one of the most important hurdles to pass to solve the worldwide energy crisis. New organic solar cells are poised to become one of the best alternative renewable energy sources because of their potential low cost, ease of processing, and compatibility with flexible substrates as compared to the expensive inorganic solar cells (Grätzel 2003, Riede *et al.* 2008, Roncali 2009, Walker *et al.* 2011). These small molecules are organic compounds (materials), each containing a delocalized Pi electron system, which can absorb sunlight, create charge carriers, and transport these charge carriers through the system (Boudreault *et al.* 2011, Krebs 2009, Smichidt-Mende *et al.* 2002, Tang 1986). The functioning and behaviors of these cells are in many ways different from those of inorganic semiconductors, as such their material properties are expected to enable a number of exciting new applications (Boudreault *et al.* 2011, Kippelen and Brédas 2009, Krebs 2009, Tang 1986). Different designs of solar cells based

---

∗Corresponding author, Ph.D., E-mail: cwpao@gate.sinica.edu.tw

on organic materials have been manufactured, examples of which include cells based on liquid crystals (Smichidt-Mende *et al.* 2002), dye sensitised solar cells (Hagfeldt and Grätzel 2000), bulk heterojunction cells (Yu and Heeger 1995), and composite cadmium/selenide polymer solar cells (Ginger and Greenham 1999). Currently, the power conversion efficiency of organic photovoltaic cells using conjugated polymers as the electron donor and fullerenes derivatives as the electron acceptor is around 10% (Chen *et al.* 2009, Wong *et al.* 2007). However, as these solar cells suffer from the problem of batch-to-batch variation in device performance due to the polydiversity of polymers, it becomes important to use an alternative electron donor. Some of the alternative electron donor materials are small molecules (Fig. 1). With molecular-level accuracy, the small molecule organic photovoltaic cells can effectively avoid the problems of batch-to-batch variation. Although, small-molecule organic photovoltaic cells are in general not as efficient as their polymer-based counterparts, these problems with efficiency have been resolved recently with the synthesis of new small molecules, the with power conversion efficiencies of which is greater than 8%, in combination with a C70 based fullerene acceptor (Scharber *et al.* 2006, Chen *et al.* 2012). The synthesis and design of new organic molecules with special properties (donor-acceptor-acceptor) are vital to the production of organic solar cells, or as a very important component in bulk heterojunction solar cells and their efficiency (Scharber *et al.* 2006, Chen *et al.* 2012). Among these types of new materials, the tailor-made small molecules A, B, A1, and B1 are promising electron donor and acceptor materials in combination with fullerenes (C60 or C70) or their derivatives used as an acceptor material (Scharber *et al.* 2006, Chen *et al.* 2012).

In this work, we systematically investigated the electronic structures, electrochemical properties, and charge carrier transport properties of A, B, A1, and B1 by carrying out a series of density functional theory (DFT) calculations. Results from our calculations on the electronic structure of singly oxidized and reduced molecules, the first anodic and cathodic potentials, and the electrochemical gaps are in accordance with those from experiments. Moreover, we estimated the electron/hole transport properties by computing the electron/hole hopping reorganization energies and transfer integrals over a wide range of molecular dimer configurations. Our calculations indicated that electron/hole hopping rates are very sensitive to the relative separations/orientations between neighboring small molecules. By analyzing the hole/electron transfer integrals from all possible molecular dimers in the molecular crystal, we also identified potential charge carrier transport bottlenecks. As we found that the hole mobilities in the molecular crystal are at least an order of magnitude higher than the electron mobilities due to high electron hopping reorganization energies, we demonstrated that these four small molecules are poor electron conducting materials.

2. Computational methods

All calculations were carried out using the Gaussian 09 and ADF 2010 packages (Gaussian 2009, ADF 2012). Geometries were optimized using DFT-B3LYP[21,22] and the 6-31G(d,p) basis sets. The transfer integrals for the nearest neighbouring molecular pairs and reorganization energies were calculated with the B3PW91,[23] B3LYP, PBEPBE,[23] LSDA,[24] LDA,[25] and GGA[26] functionals and the 6-31G(d,p) basis set, and the exchange-correlation functional of Becke and Perdew (Perdew 1986, Becke 1988), using Gaussian and ADF packages. The charge carrier mobility was calculated using the reorganization energy and transfer integral values with a better contribution from the different functionals. The small molecule electronic structure calculations in

the solution phase were performed with the Amsterdam Density Functional (ADF) 2010 package (ADF 2010) with the exchange-correlation functional of Becke and Perdew. The scalar relativistic corrections were included in the self-consistent calculation by means of the zeroth-order regular approximation (ZORA) (van Lenthe *et al.* 1993). Triple- polarization basis sets (TZP) of the Slater type were employed to describe the valence electrons of C, N, H, and S. Frozen cores consisting of a 1s shell for C, N, and S were described by means of single Slater functions. The calculation for predicting the electrochemical gaps was done in the presence of a continuous model solvent by means of the conductor-like screening model (COSMO) (Klamt and Schuumann 1993, Andzelm *et al.* 1995). The solvents used dichloromethane and tetrahydrofuran were the same as those used in the experiments.

The incoherent hopping model was employed to investigate the charge carrier mobilities of A, B, A1, and B1. The carrier mobility μ can be expressed using Einstein's relation

$$\boldsymbol{\mu} = \frac{e}{2k_bT}D \tag{1}$$

where k_b is the Boltzmann's constant, T is the temperature, e is the electronic charge, and D is the charge diffusion coefficient. This can be calculated from the hopping rate as

$$D = \frac{1}{2n}\sum_i b^2 k_i P_i; P_i = \frac{k_i}{\sum k_i} \tag{2}$$

where n is the dimensionality ($n=3$), b is the distance to the i_{th} neighbour (center of mass distance between the dimers), and k_i and P_i are the hopping rates and the relative probability for charge transfer to the i_{th} neighbour.

According to the Marcus theory (Marcus 1993), the hopping rate k_{ct} between neighbouring charge carrier occupation site X to site X_1 across the distance R_{XX1} can be expressed as follows

$$k_{ct} = \frac{2\pi}{\hbar}v^2\sqrt{\frac{1}{4\lambda\pi k_bT}}\exp\left[\frac{-(\Delta G^0 + \lambda)^2}{4\lambda k_bT}\right] \tag{3}$$

where $\hbar$, v, and λ correspond to the Planck's constant, transfer integral, and reorganization energy (Inner), respectively. $\boldsymbol{\Delta G^0}$ is the difference in the Gibbs free energy; this is equal to zero when the sites X and X_1 are the same species at zero field. From Eq. (3), it is clear that the most important parameters in determining the carrier mobilities are the internal reorganization energy λ and the transfer integral v. In this respect, lower reorganization energy and a large transfer integral would increase the charge carrier mobilities. With this method, the charge carrier mobility in a molecular single crystal can be easily evaluated.

Various computational techniques using semiempirical or *ab initio* methodologies have been created to estimate the electronic coupling V_{if} (Balzani 2001, Bixon and Jortner 1999, Newton 1991). A common method to compute V_{if} is to describe the adiabatic states of the reactants and products using a Slater determinant and to compute their splitting at the transition states (Li *et al.* 1999a). Another method is to use Koopmans' theorem to estimate the transfer integral (*t*) for holes as half splitting of the HOMO levels in a system made of two chains in the neutral state. These two methods have been used in the case of benzene and biphenyl dimers, and the two approaches give similar results, except in the strong interaction regime, an exception which is expected to take

place in the case of small molecules separated by short intermolecular distances (Pati and Karna 2001). Pati and Karna were the first to confirm the applicability of Koopmans' theorem in the study of the electron transfer (ET) in σ-bonded organic cage structures (bicyclo[1.1.1]pentane, cubane, and bicyclo[2.2.2]octane) (Wolfsberg and Helmhotz 1952). Also, the transfer integral can be estimated in a yet simpler approach from the spatial overlap between the two atomic orbitals in interaction (Pietro *et al.* 1985, Liang and Newton 1992). These considerations explain why many theoretical studies have made use of Koopmans' theorem to estimate electronic coupling (Pietro *et al.* 1985, Liang and Newton 1992, Paulson *et al.* 1996, Voityuk *et al.* 2000, Grozema *et al.* 2002, Palenberg *et al.* 2000, Valeey *et al.* 2006). For this reason, in this study we considered that much care must be taken when Koopmans' theorem is used to estimate the transfer integral in asymmetric dimers.

The theory of charge transport in organic materials relies on two contributions. The first one is the magnitude of the electronic coupling (transfer integral), which depends on the relative arrangement of the molecules in the crystal, whereas the second is the geometric relaxation of the molecule and its surrounding (reorganization energy) on movement of the charge carriers. However, Palenberg *et al.* (2000) have demonstrated that the charge transport in organic material generally based on the energy splitting in dimer method can fail, even in molecular crystal with weak van der Waals intermolecular interactions, due to the substantial impact of polarization effects, particularly on the site energies. As the transfer integral (Marcus 1993) is basically an approximation of the energetic splitting of the electronic level, in this study, we use the framework of the Marcus-Hush two-state model to calculate the electron-transfer coupling matrix element or transfer integral, V, between adjacent molecules. In these organic molecules, the highest occupied molecular orbital (HOMO) of the isolated molecule is a π orbital delocalized over the molecule (with energy ε), which for the neutral dimer is split into two levels, denoted as HOMO and HOMO-1. The coupling matrix element, *V*, is given by,

$$v = \frac{1}{2}\sqrt{(E_{HOMO} - E_{HOMO-1})^2 - (\varepsilon_2 - \varepsilon_1)^2} \tag{4}$$

In this case, the isolated molecules are identical (and in equivalent sites in the crystal), such that Eq. (4) becomes

$$v_{hole} = \frac{E_H - E_{H-1}}{2} \tag{5}$$

where E_H and E_{H-1} denote the HOMO and HOMO-1 energy levels, respectively. The transfer integral of the electron ($J_{electron}$) can be evaluated also via the energy difference between the LUMO and LUMO+1; that is,

$$v_{el} = \frac{E_{L+1} - E_L}{2} \tag{6}$$

The internal reorganization energy (Kirkpatrick 2008), λ, involves conformational changes when the molecules move from (reorganizing) neutral states to charged states, and from charged states to neutral states. The reorganization energies can be evaluated from the following equation

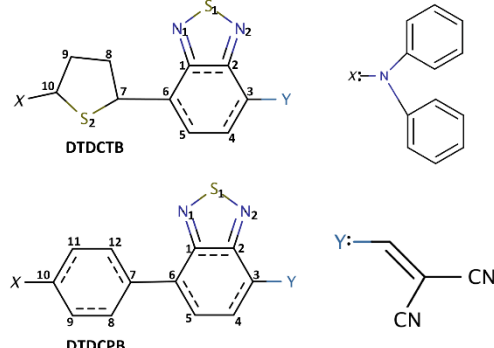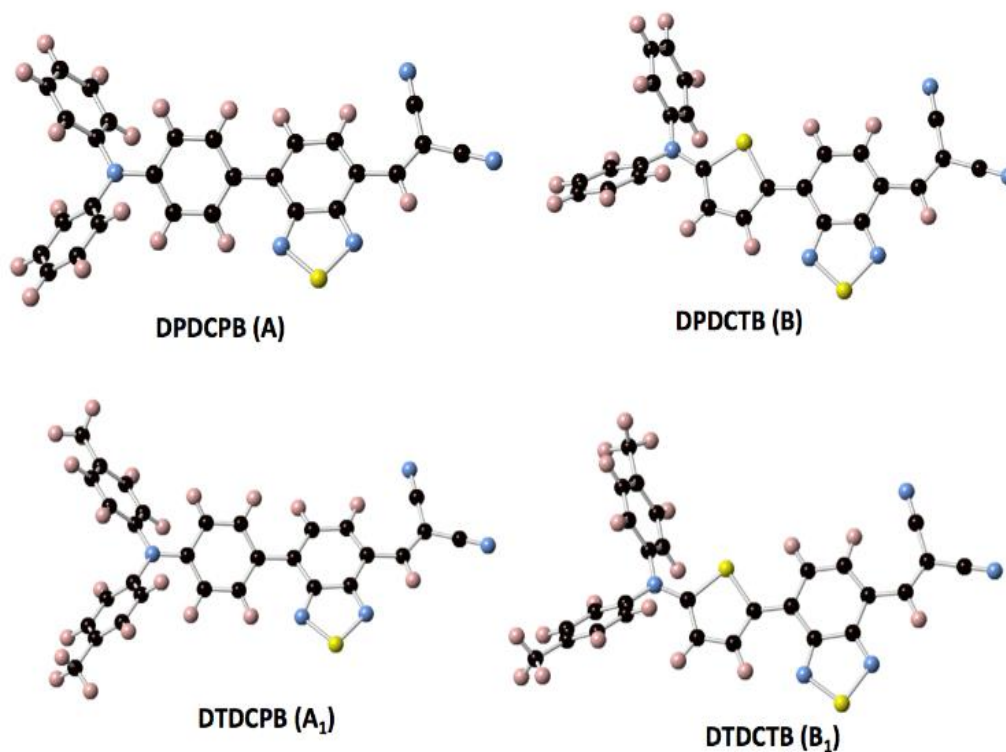$$\lambda = \lambda_1 + \lambda_2 = (E_{neu}^* - E_{ion}) + (E_{ion}^* - E_{neu}) \tag{7}$$

Fig. 1 DPDCPB (A), DPDCTB (B), DTDCPB (A1), and DTDCTB (B1) optimized structures. C, N, S, and H atoms are coloured black, blue, yellow, and pink, respectively

where λ_1 and λ_2 account for the energy difference due to the structural change of gaining and losing an electron and are equal to $E^*_{neu}-E_{ion}$ and $E^*_{ion}-E_{neu}$, respectively. Note that E^*_{neu}, E_{ion}, E^*_{ion}, and E_{neu} refer to the energies of ionized state with neutral geometry, optimized ionized geometry, neutral state with ionized geometry, and optimized neutral geometry, respectively. The reorganization energies and matrix couple element or transfer integral were calculated using the B3LYP functional; nevertheless, we also computed reorganization energies using other functionals (B3PW91, PBEPBE, LSDA, LDA, and GGA) for consistency test (see Tables 4 and 5). From Tables 4 and 5, we can find that all these functionals gave similar results on hole/electron hopping reorganization energies.

3. Results and discussions

3.1 Electronic structure

Through our calculations, we present the optimized geometries of four small molecules, A, B, A_1, and B_1. The chemical structures of these four molecules are displayed in Fig. 1. In that figure, it can be seen that A differs from A_1 in the lack of methyl groups in the external benzyl rings.

Table 1 Selected bond lengths for A, B, A$_1$, and B$_1$

	C3-C4 [a]		C4-C5 [a]		C5-C6 [a]		C6-C7 [a]		BLA [b]	
	Exp.[1]	DFT	Exp.[1]	DFT	Exp.[1]	DFT	Exp.[1]	DFT	Exp.[1]	DFT
A		1.392		1.416		1.393		1.467		
B		1.396		1.409		1.399		1.433		
A$_1$	1.379	1.392	1.407	1.415	1.376	1.393	1.472	1.466	0.030	0.023
B$_1$	1.393	1.397	1.395	1.408	1.395	1.400	1.434	1.431	0.001	0.001
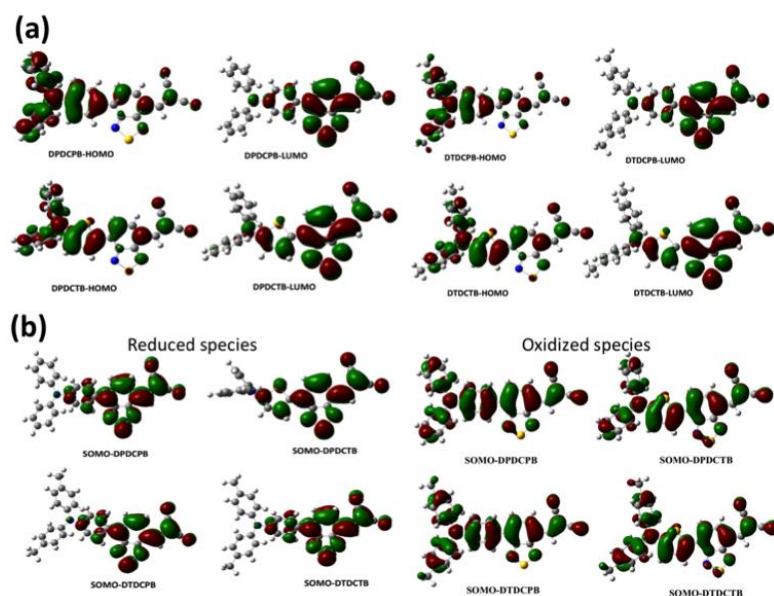
Fig. 2(a) HOMOs, LUMOs, and (b) SOMOs of DPDCPB (A), DPDCTB (B), DTDCTB (A1), and DTDCTB (B1)

Instead, we can find hydrogen atoms. The same case occurs for B and B$_1$. In contrast, A differs from B in that the central benzyl ring is replaced with the thiophene ring. The bond lengths of A, B, A$_1$, and B$_1$, determined by experiment and from DFT calculations, are listed in Table 1. The B$_1$ and A$_1$ bond lengths from our DFT calculations show excellent agreement with measurements from experiments (Chen *et al.* 2012).

Table 2 Experimental and computational band-gaps for A, B, A_1, and B_1

	HOMO[1] (eV)		LUMO[2] (eV)		$^3\Delta E^{opt}$ (eV)	
	Exp.[4]	DFT	Exp.[4]	DFT	Exp.[4]	DFT
B	-5.35	-5.42	-3.44	-3.46	1.91	2.12
B_1	-5.30	-5.32	-3.44	-3.38	1.86	2.08
A	-5.50	-5.44	-3.36	-3.49	2.14	2.12
A_1	-5.43	-5.32	-3.35	-3.44	2.08	2.05

[1]HOMO: Higher occupied molecular orbital
[2]LUMO: Lowest unoccupied molecular orbital
[3]ΔE^{opt}: Optical band-gaps
[4]Exp.: Experimental results

Table 3 Redox parameters for the molecules A, B, A_1, and B_1

	E_{ox}^1 (V)		OE_{DFT}	E_{red}^1 (V)		RE_{DFT}	ΔE^{CV} (eV)	
	Exp	DFT		Exp	DFT		Exp	DFT
B	0.41	0.58	5.38	-1.07	-1.09	-3.71	1.48	1.67
B_1	0.35	0.51	5.31	-1.09	-1.13	-3.67	1.44	1.64
A	0.60	0.67	5.47	-1.13	-1.08	-3.72	1.73	1.75
A_1	0.47	0.56	5.36	-1.19	-1.11	-3.69	1.66	1.67

E_{ox}: Oxidation Potential
OE_{DFT}: Oxidation Energy
E_{red}: Reduction Potential
RE_{DFT}: Reduction Energy
ΔE^{CV}: Cyclic Voltammogram Band-gaps
Exp.: Experimental results
DFT: Density Functional theory results

The HOMOs, LUMOs, and SOMOs (Singly Occupied Molecular Orbitals) of the molecules A, B, A_1, and B_1 are displayed in Fig. 2. Electronic structure analysis shows that the HOMOs (Fig. 2(a)) are mainly localized on the benzene rings; in contrast, the LUMOs (Fig. 2(a)) are mainly localized on the iso-indene or benzothiophene (BT) rings. Hence, when the molecules are oxidized, the electrons are removed from the benzene rings, whereas the incoming electrons are likely to be found in the iso-indene structures when the molecules are reduced.

The electronic structures for A, B, A_1, and B_1 can be further elucidated by analysing their corresponding SOMOs (Fig. 2(b)). Note that the SOMOs for all four small molecules in reduced states are very similar to the LUMOs in the neutral molecules, an observation confirming that the electrons can be found in the iso-indene structure. The SOMOs in the reduced species show an important contribution from the iso-indene structures. The SOMOs of the oxidized species, however, are very similar to the HOMOs in the neutral molecules A, B, A_1, and B_1. These orbitals receive contributions from the whole molecule, particularly from their benzene rings. Therefore, for all four small molecules, oxidation takes place in the entire molecule, especially in the benzene rings.

Tables 2 and 3 list the band-gaps (Table 2) and the oxidation free energies (Table 3) from experiments and DFT calculations for A, B, A_1 and B_1, as well as the first anodic and cathodic

potentials, referred to as the ferrocenium/forrocene (Fc$^+$/Fc) potentials, which have been derived from the free energies. As expected from the relatively low LUMOs, the computed $\mathbf{\Delta G^0}$ values for the reduction processes, -1.09 eV (B), -1.13 eV (B$_1$), -1.08 eV (A), and -1.11 eV (A$_1$), are exothermic. The corresponding cathodic potentials, 0.58 V (B), 0.51 V (B$_1$), 0.67 V (A), and 0.56 V (A$_1$), are in concordance with the experimental values of 0.41 V, 0.35 V, 0.60 V, and 0.47 V, respectively. As expected from the quite deep HOMOs, the computed free energies for the oxidation processes are very endothermic (5.38 eV, 5.31 eV, 5.47 eV, and 5.36 eV). The deviations in the predicted oxidation potentials with respect to the observed ones are also quite small. The electrochemical gaps (EC) for the four molecules are approximately 13% smaller for B and B$_1$, and 2% smaller for A and A$_1$. The predicted EC gaps for A, B, A$_1$ and B$_1$ are in good agreement with experiments.

The electrochemical gaps for A, B, A$_1$, and B$_1$ can also be evaluated from the HOMO-LUMO gaps in the neutral molecules (Table 2). It is worth noting that the reduction energy and oxidation energy can also explain the main differences between the redox properties of the four molecules; molecule B$_1$ is reduced and oxidized somewhat more easily than are B, A, and A$_1$. In addition, other computational studies show similar band-gap results in B$_1$, bithiopheneide-Dithienosilole/Dithienogermole copolymers, and Thieno [3,4-c]pyrrole-4,6-dione analogues (Lin *et al.* 2011, Boudreault *et al.* 2007). Chen *et al.* (2012) found that the band-gap value according to the HOMO-LUMO level is 2.01 eV for DTDCTB. This result is quite consistent with our result from DFT calculation, 2.05 eV. Marks *et al.* (2005) found values between 2.79 and 3.13 eV for a series of molecules with characteristics similar to those of A, B, A$_1$, and B$_1$. Thus, it appears that our results are consistent with those of other computational studies of small molecules.

3.2 Reorganization energies

Tables 4 and 5 present the reorganization energies (λ) from the computational results according to different functionals for the hole and electron hopping of A, B, A$_1$, and B$_1$. In all cases, it can be observed in general that B and B$_1$ have the highest reorganization energies for the hole and electron hopping. Note that according to the DFT results, the reorganization energies for electron hopping are several times higher than those for hole hopping, demonstrating that all four small molecules are poor electron conducting materials. Our results shows that the reorganization energies for A, B, A$_1$, and B$_1$ are very similar to the reorganization energies of naphthalene, anthracene, tetracene, and pentacene (0.189 eV, 0.143 eV, 0.121, and 0.099 eV, respectively) (Deng and Goddard 2004). In contrast, these reorganization energies are 50% lower than those of Alq3 and their derivatives (Wang *et al.* 2013), and between 70% to 80% lower in the case of DSA and their derivatives (Lee *et al.* 2012). In the case of the reorganization energy and the number of phenyl rings in the molecular structure, according to Deng and Goddard 2004, these results show good similarity with the results published for naphthalene, anthracene, tetracene, and pentacene. Our computational calculations show that the reorganization energies for B and B$_1$ (three phenyl rings) are higher than those for A and A$_1$ (four phenyl rings) as a result of the greater number of phenyl rings, even though the variation in the values of the reorganization energies for the compound with the same number of phenyl rings are small. It is interesting to note that, when the methyl groups in A$_1$ are replaced with hydrogen atoms (i.e., A), the reorganization energy for hole hopping drops by 0.023 eV, while the electron hopping reorganization energy increases by 0.002 eV. In contrast, for B$_1$, when the methyl radicals are replaced with hydrogen atoms, its reorganization energy increases by 0.031 eV, while that for electron hopping increases by 0.016

Table 4 Reorganization energies (eV) for the molecules A, B, A_1, and B_1 (hole hopping)

	λ_{Tot} PW91	λ_{Tot} B3LYP	λ_{Tot} PBEPBE	λ_{Tot} LDA	λ_{Tot} GGA
A	0.098	0.094	0.093	0.083	0.080
B	0.165	0.162	0.163	0.155	0.142
A_1	0.116	0.117	0.118	0.123	0.118
B_1	0.133	0.131	0.133	0.144	0.137

Table 5 Reorganization Energies (eV) for the molecules A, B, A_1, and B_1 (electron hopping)

	λ_{Tot} PW91	λ_{Tot} B3LYP	λ_{Tot} PBEPBE	λ_{Tot} LDA	λ_{Tot} GGA
A	0.364	0.361	0.362	0.354	0.347
B	0.452	0.454	0.455	0.446	0.456
A_1	0.360	0.359	0.359	0.348	0.343
B_1	0.436	0.438	0.439	0.437	0.436
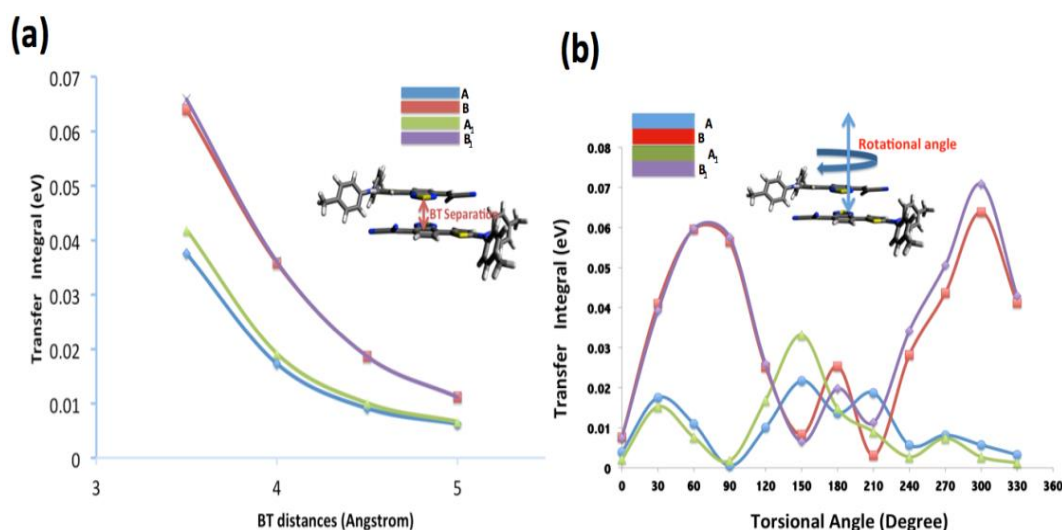
Fig. 3 Hole transfer Integral: (a) as the function of separations between two BT rings, and b) Transfer Integral vs. Torsional Angle in dimer A, B, A_1, and B_1

eV. The effect of the methyl substitution on reorganization energy is significant according to the electronic characteristics of the original systems. A possible explanation is that the substitution could promote intramolecular charge transfer due to the network of the electron donating methyl group (Sun *et al.* 2012), which is not the case for A and A_1.

3.3 Dependencies of transfer integrals and molecular dimer geometries

From Eq. (3), we can discover that the charge carrier hopping rates between molecular dimers of the same molecules depend only on the transfer integrals. According to our results, the transfer integrals between different molecular dimers of A, B, A_1, and B_1 are very sensitive to their relative molecular separations and orientations (Fig. 3). In this subsection, we systematically discuss the
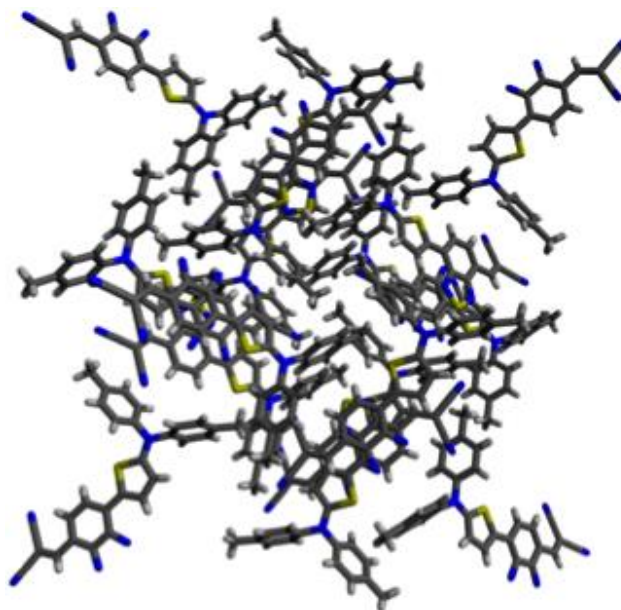
Fig. 4 Crystal configuration of B_1

correlations between transfer integrals and molecular dimer-related separations/orientations. Fig. 3(a) shows the hole transfer integrals as a function of separations between the BT rings of two molecules in the crystal packing configurations reported in Chen *et al.* 2012. From Fig. 3(a), it is clear that B/B1 have higher transfer integrals than A/A$_1$. It can also be observed that the transfer integrals undergo significant drops with respect to increasing BT ring separations, implying that large intermolecular separation leads to low hole hopping rates (and mobilities). Next, we examined the effects of relative molecular orientations on the hole transfer integrals by rotating one small molecule around an axis normal to the BT ring planes (inset, Fig. 3(b)). Note that the BT separations between the two molecules were fixed at 6 Å (inset, Fig. 3(b)). Fig. 3(b) displays the transfer integrals for hole transport as a function of relative rotation angle τ, and from Fig. 3, we can see that the transfer integrals are very sensitive to their relative orientations and that the transfer integrals of B/B$_1$ are generally higher than those of A/A$_1$. The magnitudes of hole transfer integrals with respect to torsional angles between two small molecules are compiled in Table S1 in the Supporting Information. Interestingly, a previous study indicated that the antiparallel, cofacial packing between two small molecules (corresponding to τ=0) might facilitate charge carrier hopping; however, our calculations indicate that molecular dimers at τ=0 have almost the lowest transfer integrals, implying that this antiparallel, cofacial packing might not be the preferential pathway for charge carrier hopping.

3.4 Charge carrier transfer in molecular crystal

The charge transport properties of organic molecules are significantly affected by the relative orientations and crystal packing motifs. Based on crystal structures of these compounds, we investigated the charge carrier transport properties in the molecular crystal of all four small molecules. One molecule was chosen as the charge donor, and all the nearest neighbour molecules
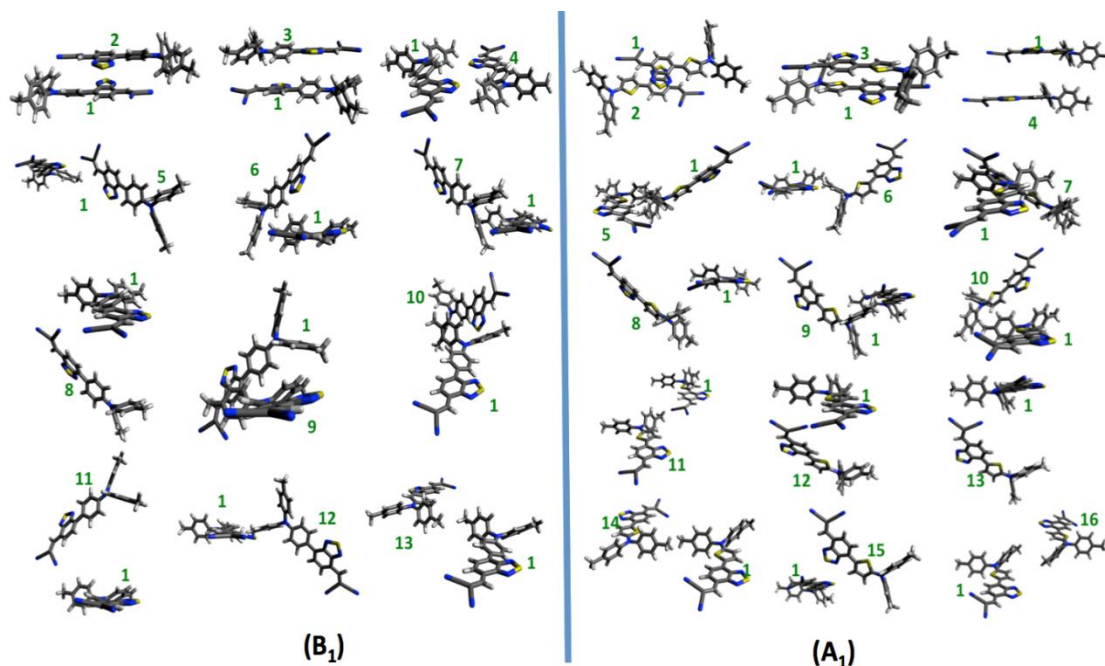
Fig. 5 Molecular pairs in the partial molecular packing of B_1 and A_1
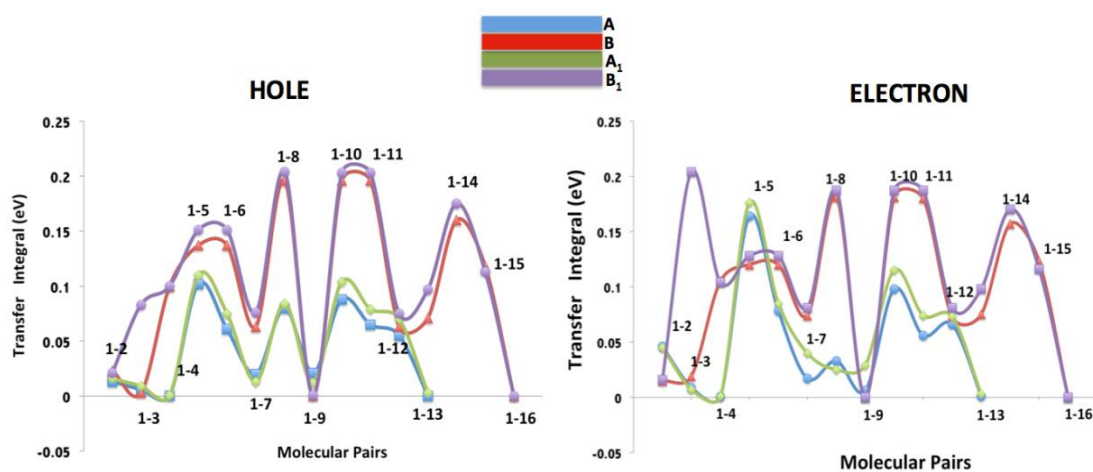
Fig. 6 Transfer integral (hole and electron) for the dimers A, B, A_1, and B_1 according to the molecular pairs (eV) in the full molecular packing

could be regarded as the charge acceptor. The crystal structures were based on those of the A_1 and B_1 extracted from XRD data (Chen *et al.* 2012) (Fig. 4). We focused on the substitution effect on transfer integrals under the assumption that the derivatives A and B have the same crystal parameters as those of DTDCTB and DTDCPB. Because the charge carrier mobilities in molecular crystals are highly anisotropic, we must consider all of the possible nearest molecular pairs of all four small molecules. Fig. 5 illustrates all possible nearest neighbour pairs of B_1/B (left panel) and A_1/A (right panel). Note that totals of fifteen and twelve molecular dimer configurations were

identified in B_1/B and A_1/A molecular crystals, respectively.

Fig. 6 displays the respective transfer integrals for the molecular dimers shown in Fig. 5. The magnitudes of these transfer integrals are provided in Tables S2 and S3 in the Supporting Information. Note that the magnitudes of the transfer integrals of A, B, A_1, and B_1 range between 0.0001 to 0.204 eV (Hole), and 0.0001 to 0.187 eV (Electron), respectively, which demonstrates that the hole/electron hopping rates are highly anisotropic, and molecular pairs with low transfer integrals (e.g., pairs 1-2, 1-3, and 1-4) could potentially become bottlenecks for charge carrier transport in the molecular crystal. From the hole transfer integrals summarized in table S5, it can be seen that the most important hole-transport pathways present are 1-5 for A, 1-11 for B, 1-6 for A_1, and 1-14 for B_1. These transfer integrals are much larger than those in other dimers in all four types of molecules, which indicates that the 1-5 (A), 1-11 (B), 1-6 (A_1), and 1-14 (B_1) directions are the dominant conducting channels. However, due to the different intermolecular distances among the different dimers, there are obvious differences among the hole/electron transfer integral. The transfer integral variations for the various dimers are small (Tables S7, S8, S9, and S10) when small substituents are introduced to A_1 and B_1. For A_1, the transfer integrals of both hole and electron in pathway 1-11 are very high (7.4×10^{-3} and 0.074 eV respectively), demonstrating that the transfer integral may exhibit high charge mobilities for holes. When the methyl radicals are replaced with H atoms, the center of mass distance and nearest distance are similar, whereas the planar angle becomes a little bit smaller (51.52 to 49.42°). We can observe the same behaviour with the values of the transfer integral (7.4×10^{-3} to 7.8×10^{-3} eV). According to our results, the transfer integral shows small changes when the methyl radicals are replace by H atoms. These small changes can be appreciated by means of the average for the different molecules. It can be seen that for A1, the average of the transfer integral for all the dimer is 3.09×10^{-3} eV, whereas for A, it is 2.83×10^{-3} eV. The transfer integral decreases by 2.6×10^{-4} eV. In the case of B1, we can observe a transfer integral decrease of 2.17×10^{-2} to 1.53×10^{-2} eV in B. This decrease is around $6.4E^{-3}$ eV. All these changes in the values of the transfer integral show very small variation, considering the susceptibility of these values with the distances and the displacements. But it is not only the values of transfer integral that undergo a very small change. The values of the centre of mass distance, planar angle, and nearest atoms distances are also affected by the introduction of H atoms. It can be seen that the average for the values of the planar angle in A1 is 35.26°, whereas in A, it is 34.12°. For centre of mass distance, we can observe that the average in A_1 is 11.7 Å, while in A, it is 11.23 Å. In the case of the nearest atoms distance, the variations are almost negligible because the average of the distances in A_1 is 3.33 Å, whereas for A it is 3.35 Å. These results in A_1 and A are similar to the results or variations that are observe in the molecules of B_1 and B.

In general, the transfer integrals of B and B_1 are higher than those of A and A_1, which can be attributed to the higher density of B/B_1 crystal relative to A/A_1 (Chen *et al.* 2012), thereby leading to smaller intermolecular separation and higher transfer integrals. These values for the transfer integrals of A, B, A_1, and B_1 are in the same range as the values calculated for naphthalene, anthracene, tetracene, pentacene, DSA, Alq3, and their derivatives (Lin *et al.* 2011, Boudreault *et al.* 2007, Deng and Goddard 2004). For naphthalene, anthracene, tetracene, and pentacene, the transfer integrals are all in the range of 0.0008 to 0.13 eV. For Alq3 and their derivatives, the transfer integral values are between 0.00 to 0.50 eV. In contrast, for DSA and its derivatives, the values are between 9.2×10^{-8} to 0.09 eV. According to these values, the charge carrier mobilities in the different compounds of A, B, A_1, and B_1 are dependent on the number of pairs in the crystal structure, making the number of pairs a critical factor for determining the charge carrier mobility.

The charge carrier mobilities μ of the four small molecules were estimated from Eqs. (1)-(7)

Table 6 Hole and electron mobilities (μ) in the crystal structures

	A	B	A_1	B_1
μ_{hole} (cm^2/V s)	0.085	0.128	0.073	0.198
$\mu_{electron}$ (cm^2/V s)	0.0074	0.0041	0.0087	0.0052
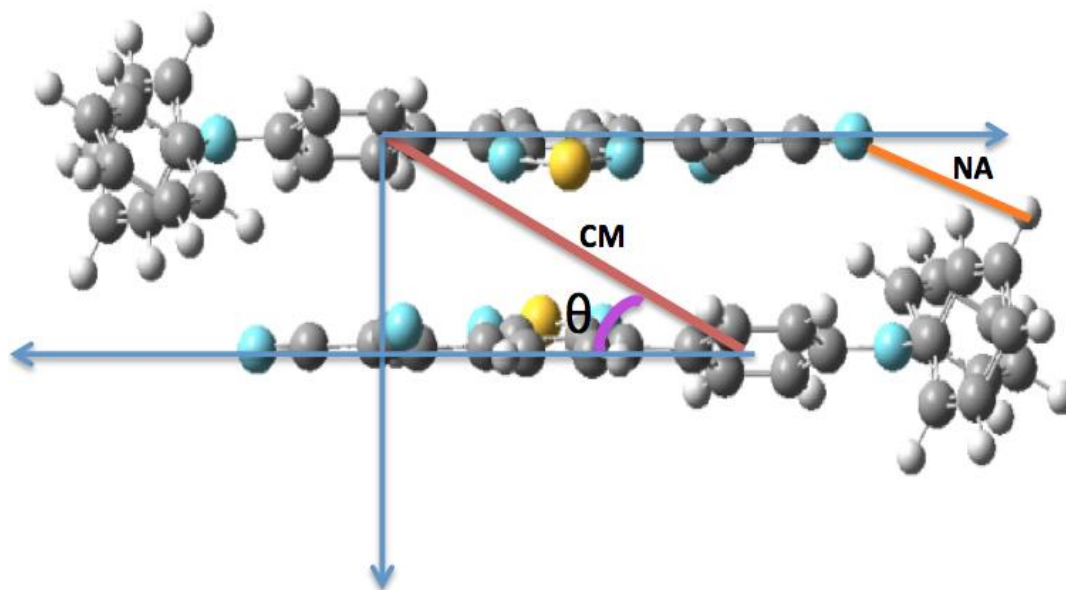
Fig. 7 Planar angle (θ), Center of mass (CM) distance, and nearest distance (NA) For the different dimer

using reorganization energies and transfer integrals obtained from previous QM calculations. The hole/electron mobilities of A_1 and B_1 in the crystal structures are presented in Table 6. It can be clearly seen that the charge carrier mobilities of the holes increase in A_1 when the methyl radicals are replaced by H atoms, whereas in B_1, they decrease. The charge carrier mobility of electrons in both cases decrease when the methyl radical are replaces by H atoms. If we analyse the results according to charge carrier mobility values, we can see that our charge carrier mobilities are lower than the charge carrier mobility of anthracene (0.54 cm^2/V s), results that are in general similar to those of DSA, DSA-CN, DSA-OCH$_3$, and DSA-TBU (0.21, 0.14, 0.0026, and 0.045 cm^2/V s, respectively), and lower than that of Alq3 (Lin *et al.* 2011, Boudreault *et al.* 2007, Deng and Goddard 2004). One important observation from Table 6 is that the hole mobilities are at least an order of magnitude higher than those of the electrons. Note that from Figs. 5 and 6, it is evident that the hole/electron transfer integrals have similar magnitudes, showing that, it is the high reorganization energies for electron hopping from our calculations (Table 5) that lead to low electron mobilities in these small molecules. Therefore, our calculations demonstrate that all four small molecules are poor electron conducting materials. Next, we find that the hole mobilities of B and B_1 are higher than those of A and A_1, which can be attributed to the noticeably higher hole transfer integrals of B and B_1 (Fig. 6). In addition, from Eq. (2), it is clear that the diffusion constant monotonically increases with increasing nearest neighbour pairs. In B/B_1 molecular crystals, we can identify fifteen nearest molecular pairs, in contrast to twelve nearest neighbors in A/A_1 molecular crystals, thereby leading to higher diffusion constants in B/B_1 than in A/A_1.

A recent study shows that the zero field hole mobilities of A_1 from an OPV device fabricated using vacuum co-deposition were several orders of magnitude lower than those estimated in the present study (Chen *et al.* 2012). We attribute this to differences in the microstructures of the molecular films. In the present study, the whole molecular film was one single molecular crystal without any defects; however, in experiments, the films were fabricated using vacuum co-deposition of A_1 and C_{70} simultaneously, which may have led to highly-disordered film microstructures filled with defects and consequently substantially lower hole mobilities. The effects of defects and large-scale disorder on charge carrier mobilities can be evaluated by carrying out kinetic Monte Carlo charge carrier dynamics simulations (Rühle *et al.* 2011, Nelson *et al.* 2009), which will be our next step in studying the charge carrier dynamics of small molecule thin films.

4. Conclusions

We have carried out a series of *ab initio* calculations to investigate the electronic structures, electrochemical properties, and charge carrier transport properties of new tailor-made small-molecule electron donor molecules, A, B, A_1, and B_1. Our results from the calculations on the electronic structures and electrochemical properties of these small molecules are in concordance with those from experiments. Our calculations reveal that the hole/electron hopping rates are extremely sensitive to the relative orientations and separations between neighbouring molecules, and that the antiparallel, cofacial packing molecular dimer configurations are not the most favourable charge carrier transport path. It was predicted that A, B, A_1, and B_1 would show high charge mobilities. According to our calculations, the principals hole transport pathways are 1-5(A), 1-11 (B), 1-6 (A_1), and 1-14 (B_1), whereas in the electron, the principal transport pathways are 1-5 (A), 1-8 and 1-10 (B), 1-5 (A_1), and 1-3 (B_1). The different DFT calculations showed that the reorganization energy of A in the hole increases when the methyl groups are present, such that this compound becomes A_1. In contrast, for B, the reorganization energy decreases when this compound becomes B_1 due to the presence of methyl groups. In the case of the reorganization energy in the electron, we can see decreases in both cases when the methyl groups are present in the structures. For A and A_1, the lower reorganization energies and the high transfer integrals lead to mobilities of 0.085 and 0.073 cm^2/V s in the hole, while those in the electron are 0.0074 and 0.0087 cm^2/V s, respectively. We can observe very small variations in the planar angle, centre of mass distances, and nearest atom distances when the methyl radicals are replaced by H atoms, but these very small variations do not significantly affect the values of the different transfer integrals in the dimers. For that reason, the mobilities of the different molecules are mainly affected by reorganization energy, although the variance in the mobility is quite small. We can see that hole mobility decreases when the methyl groups are present in the structure, whereas electron mobility increases. For B and B_1, the hole and electron mobilities are 0.128 and 0.198 cm^2/V s in the hole, while those in the electron are 0.0041 and 0.0052 cm^2/V s. These values indicate that the hole and electron mobility increase when the methyl group is present in the structure. Finally, our calculations indicate that the hole mobilities of these four small molecules are at least an order of magnitude higher than the electron mobilities due to the high reorganization energies for electron hopping. On the basis of these details calculations, we draw the conclusion that because of their low conductivity, the new tailor-made molecules (A, B, A_1, B_1) have wide application prospects as promising novel donor materials for small-molecule solar cells.

Acknowledgments

References

Andzelm, J., Kölmel, C. and Klamt, A. (1995), "Incorporation of solvent effects into density functional calculations of molecular energies and geometries", *J. Chem. Phys.*, **103**(21), 9312-9320.

Balzani, V. (2001), *Electron Transfer in Chemistry*, Wiley-VCH, Weinheim, Germany.

Becke, A.D. (1988), "Density-functional exchange-energy approximation with correct asymptotic behavior", *Phys. Rev. A*, **38**(6), 3098-3100.

Becke, A.D. (1993), "Density-functional thermochemistry. III. The role of exact exchange", *J. Chem. Phys.*, **98**(7), 5648-5652.

Becke, D. (1993), "A new mixing of hartree-fock and local density-functional theories", *J. Chem. Phys.*, **98**(2), 1372-1377.

Bixon, M. and Jortner, J. (1999), "Electron transfer: From isolated molecules to biomolecules", *Adv. Chem. Phys.*, **106-107**.

Boudreault, P., Wakim, S., Blouin, N., Simard, M., Tessier, C.H., Tao, Y. and Leclerc, M. (2007), "Synthesis, characterization and application of indolo[3,2-*b*]carbazole semiconductors", *J. Am. Chem. Soc.*, **129**(29), 9125-9136.

Boudreault, P.L.T., Najari, A. and Leclerc, M. (2011), "Processable low-bandgap polymers for photovoltaic applications", *Chem. Mater.*, **23**(3), 456-469.

Chen, H.Y., Hou, J., Zhang, S., Liang, Y., Yang, G., Yang, Y., Yu, L., Wu, Y. and Li, G. (2009), "Polymer solar cells with enhanced open-circuit voltage and efficiency", *Nat. Photon.*, **3**(11), 649-653.

Chen, Y.H., Lin, L.Y., Lu, C.W., Lin, F., Huang, Z.Y., Lin, H.W., Wang, P.H., Liu, Y.H., Wong, K.T., Wen, J., Miller, D.J. and Darling, S.B. (2012), "Vacuum-deposited small-molecule organic solar cells with high power conversion efficiencies by judicious molecular design and device optimization", *J. Am. Chem. Soc.*, **134**(33), 13616-13623.

Deng, W.Q. and Goddard III, W.A. (2004), "Predictions of hole mobilities in oligoacene organic semiconductors from quantum mechanical calculations", *J. Phys. Chem. B*, **108**(25), 8614-8621.

Gaussian 09, Revision D.01, Frisch, G.W., Trucks, H.B., Schlegel, G.E., Scuseria, M.A., Robb, J.R., Cheeseman, G., Scalmani, V., Barone, B., Mennucci, G.A., Petersson, H., Nakatsuji, M., Caricato, X., Li, H.P., Hratchian, A.F., Izmaylov, J., Bloino, G., Zheng, J.L., Sonnenberg, M., Hada, M., Ehara, K., Toyota, R., Fukuda, J., Hasegawa, M., Ishida, T., Nakajima, Y., Honda, O., Kitao, H., Nakai, T., Vreven, J.A., Montgomery, J.J.E., Peralta, F., Ogliaro, M., Bearpark, J.J., Heyd, E., Brothers, K.N., Kudin, V.N., Staroverov, R., Kobayashi, J., Normand, K., Raghavachari, A., Rendell, J.C., Burant, S.S., Iyengar, J., Tomasi, M., Cossi, N., Rega, J.M., Millam, M., Klene, J.E., Knox, J.B., Cross, V., Bakken, C., Adamo, J., Jaramillo, R., Gomperts, R.E., Stratmann, O., Yazyev, A.J., Austin, R., Cammi, C., Pomelli, J.W., Ochterski, R.L., Martin, K., Morokuma, V.G., Zakrzewski, G.A., Voth, P., Salvador, J.J., Dannenberg, S., Dapprich, A.D., Daniels, Ö., Farkas, J.B., Foresman, J.V., Ortiz, J., Cioslowski, D.J. and Fox, G. Wallingford, C.T. (2009).

Ginger, D.S. and Greenham, N.C. (1999), "Charge separation in conjugated-polymer/nanocrystal blends", *Synt. Met.*, **101**(1), 425-428.

Grätzel, M. (2003), **"**Dye-sensitized solar cells", *J. Photochem. Photobio. C: Photochem. Rev.*, **4**(2), 145-153.

Grozema, F.C., Van Duijnen, P.T., Berlin, Y.A. and Ratner, S.M.A.L.D.A. (2002), "Intramolecular charge transport along isolated chains of conjugated polymers: Effect of torsional disorder and polymerization

defects", *J. Phys. Chem. B*., **106**(32), 7791-7795.

Hagfeldt, A. and Gratzel, M. (2000), "Molecular photovoltaics", *Acc. Chem. Res*., **33**(5), 269-277.

Huang, F., Chen, K.S., Yip, H.L., Hau, S.K., Acton, O., Zhang, Y., Luo, J. and Jen, A.K.Y. (2009), "Development of new conjugated polymers with donor-pi-bridge-acceptor side chains for high performance solar cells", *J. Am. Chem. Soc*., **131**(39), 13886-13887.

Hutchison, G.R., Ratner, M.A. and Marks, T.J. (2005), "Intermolecular charge transfer between heterocyclic oligomers. Effects of heteroatom and molecular packing on hopping transport in organic semiconductors", *J. Am. Chem. Soc*., **127**(48), 16866-16881.

Kippelen, B. and Brédas, J.L. (2009), "Organic photovoltaics", *Energy Environ. Sci*., **2**(3), 251-261.

Kirkpatrick, J. (2008), "An approximate method for calculating transfer integrals based on the ZINDO Hamiltonian", *Int. J. Quantum Chem*., **108**(1), 51-56.

Klamt, A. and Schüümann, G. (1993), "COSMO: A new approach to dielectric screening in solvents with explicit expressions for the screening energy and its gradient", *J. Chem. Soc. Perkin Trans*., **2**(5), 799-805.

Krebs, F.C. (2009), "Fabrication and processing of polymer solar cells: A review of printing and coating techniques", *Sol. Energy Mater. Sol. Cell*., **93**(4), 394-412.

Lee, C., Yang, W. and Parr, R.G. (1988), "Development of the colle-salvetti correlation-energy formula into a functional of the electron density", *Phys. Rev. B*, **37**(2), 785-789.

Lee, H., Jeong, K., Cho, S.W. and Yi, Y. (2012), "Theoretical study on the effects of nitrogen and methyl substitution on tris-(8-hydroxyquinoline) aluminum: An efficient exciton blocking layer for organic photovoltaic cells", *J. Chem. Phys*., **137**(3), 034704.

Li, X.Y. and He, F.C. (1999b), "Electron transfer between biphenyl and biphenyl anion radicals: Reorganization energies and electron transfer matrix elements", *J. Comput. Chem*., **20**(6), 597-603.

Li, X.Y., Tang, X.S. and He, F.C. (1999a), "Electron transfer in poly (*p*-phenylene) oligomers: Effect of external electric field and application of Koopmans theorem", *Chem. Phys*., **248**(2-3), 137-146.

Liang, C. and Newton, M.D. (1992), "Ab initio studies of electron transfer: Pathway analysis of effective transfer integrals", *J. Phys. Chem*., **96**(7), 2855-2866.

Liang, Y., Xu, Z., Xia, J., Tsai, S.T., Wu, Y., Li, G. and Yu, L. (2010), "For the bright future-bulk heterojunction polymer solar cells with power conversion efficiency of 7.4%", *Adv. Mater*., **22**(20), E135-E138.

Lin, L.Y., Chen, Y.H., Huang, Z.Y., Lin, H.W., Chou, S.H., Lin, F. and Wong, K.T. (2011), "A low-energy-gap organic dye for high-performance small-molecule organic solar cells", *J. Am. Chem. Soc*., **133**(40), 15822-15825.

Marcus, R.A. (1993), "Electron transfer reactions in chemistry", *Rev. Mod. Phys*., **65**(3), 599-610.

Nelson, J., Kwiatkowski, J.J., Kirkpatrick, J. and Frost, J.M. (2009), "Modeling charge transport in organic photovoltaic materials", *Acc. Chem. Res*., **42**(11), 1768-1778.

Newton, M.D. (1991), "Quantum chemical probes of electron-transfer kinetics: The nature of donor-acceptor interactions", *Chem. Rev*., **91**(5), 767-792.

Palenberg, M.A., Silbey, R.J., Malagoli, M. and Bredas, J.L. (2000), "Almost temperature independent charge carrier mobilities in liquid crystals", *J. Chem. Phys*., **112**(3), 1541-1546.

Pati, R. and Karna, S.P. (2001), "Ab initio hartree-fock study of electron transfer in organic molecules", *J. Chem. Phys*., **115**(4), 1703-1715.

Paulson, B.P., Curtiss, L.A., Bal, B., Closs, G.L. and Miller, J.R. (1996), "Investigation of through-bond coupling dependence on spacer structure", *J. Am. Chem. Soc*., **118**(2), 378-387.

Perdew, J.P. (1986), "Density-functional approximation for the correlation energy of the inhomogeneous electron gas", *Phys. Rev. B*, **33**(12), 8822-8824.

Perdew, J.P. and Wang, Y. (1992), "Accurate and simple analytic representation of the electron-gas correlation energy", *Phys. Rev. B*, **45**(23), 13244-13249.

Perdew, J.P., Burke, K. and Ernzerhof, M. (1996), "Generalized gradient approximation made simple", *Phys. Rev. Lett*., **77**(18), 3865-3868.

Pietro, W.J., Marks, T.J. and Ratner, M.A. (1985), "Resistivity mechanisms in phthalocyanine-based linear-

chain and polymeric conductors: Variation of bandwidth with geometry", *J. Am. Chem. Soc.*, **107**(19), 5387-5391.

Riede, M., Mueller, T., Tress, W., Schueppel, R. and Leo, K. (2008), "Small-molecule solar cells-status and perspectives", *Nanotech.*, **19**(42), 424001.

Roncali, J. (2009), "Molecular bulk heterojunctions: An emerging approach to organic solar cells", *Acc. Chem. Res.*, **42**(11), 1719-1730.

Rühle, V., Lukyanov, A., May, F., Schrader, M., Vehoff, T., Kirkpatrick, J. and Andrienko, D. (2011), "Microscopic simulations of charge transport in disordered organic semiconductors", *J. Chem. Theo. Comput.*, **7**(10), 3335-3345.

Scharber, M.C., Mühlbacher, D., Koppe, M., Denk, P., Waldauf, C., Heeger, A.J. and Brabec, C.J. (2006), "Design rules for donors in bulk-heterojunction solar cells-towards 10% energy-conversion efficiency", *Adv. Mater.*, **18**(6), 789-794.

Smichidt-Mende, L., Fechtenkotter, A., Mullen, K., Friend, R.H. and Mackenzie, J.D. (2002), "Efficient organic photovoltaics from soluble discotic liquid crystalline materials", *Phys. E*, **24**(1-2), 263-267.

Sun, Y., Welch, G.C., Leong, W.L., Yakacs, C.J., Bazan, G.C. and Heeger, A.J. (2012), "Solution-processed small-molecule solar cells with 6.7% efficiency", *Nat. Mater.*, **11**(1), 44-48.

Tang, C.W. (1986), "Two-layer organic photovoltaic cell", *Appl. Phys. Lett.*, **48**(2), 183-185.

Valeev, E.F., Coropceanu, V., Da Silva Filho, D.A., Salman, S. and Brédas, J.L. (2006), "Effect of electronic polarization on charge-transport parameters in molecular organic semiconductors", *J. Am. Chem. Soc.*, **128**(30), 9882-9886.

Van Lenthe, E., Baerends, E.J. and Snijders, J.G. (1993), "Relativistic regular two-component Hamiltonians", *J. Chem. Phys.*, **99**(6), 4597-4610.

Voityuk, A.A., Rosch, N., Bixon, M. and Jortner, J. (2000), "Electronic coupling for charge transfer and transport in DNA", *J. Phys. Chem. B*, **104**(41), 9740-9745.

Vosko, S.H., Wilk, L. and Nusair, M. (1980), "Accurate spin-dependent electron liquid correlation energies for local spin density calculations: a critical analysis", *Can. J. Phys.*, **58**(8), 1200-1211.

Walker, B., Kim, C. and Nguyen, T.Q. (2011), "Small molecule solution-processed bulk heterojunction solar cells", *Chem. Mater.*, **23**(3), 470-482.

Wang, L., Xu, B., Zhang, J., Dong, Y., Wen, S., Zhang, H. and Tian, W. (2013), "Theoretical investigation of electronic structure and charge transport property of 9,10-distyrylanthracene (DSA) derivatives with high solid-state luminescent efficiency", *Phys. Chem. Chem. Phys.*, **15**(7), 2449-2458.

Wolfsberg, M. and Helmhotz, L. (1952), "The spectra and electronic structure of the tetrahedral ions MnO_4^-, CrO_4^{--}, and ClO_4", *J. Chem. Phys.*, **20**(5), 837-843.

Wong, W.Y., Wang, X.Z., He, Z., Djurišić, A.B., Yip, C.T., Cheung, K.Y. and Chan, W.K. (2007), "Metallated conjugated polymers as a new avenue towards high-efficiency polymer solar cells", *Nat. Mater.*, **6**(7), 521-527.

Yu, G. and Heeger, A.J. (1995), "Charge separation and photovoltaic conversion in polymer composites with internal donor/acceptor heterojunctions", *J. Appl. Phys.*, **78**(7), 4510-4515.

DC

Appendix

Table S1 Reorganization energy (eV) for the molecules A, B, A1, and B1 (B3LYP)

	Hole Hopping		
	$^1\lambda_N$	$^2\lambda_C$	$^3\lambda_{Tot}$
A	0.049	0.045	0.094
B	0.083	0.079	0.162
A_1	0.061	0.056	0.117
B_1	0.065	0.066	0.131

Table S2 Reorganization energy (eV) for the molecules A, B, A1, and B1 (B3LYP)

	Electron Hopping		
	λ_N	λ_C	λ_{Tot}
A	0.178	0.183	0.361
B	0.222	0.232	0.454
A_1	0.178	0.182	0.359
B_1	0.231	0.207	0.438

Table S3 Transfer integral (hole) of A, B, A1, and B1 according to torsional angle (degree). BT distances=6.0 A (B3LYP)

Comp/Ang	A	B	A_1	B_1
0	0.00393	0.00762	0.00218	0.00748
30	0.01749	0.04095	0.01523	0.03918
60	0.01098	0.05959	0.00762	0.05972
90	0.00054	0.05646	0.00177	0.05755
120	0.01003	0.02517	0.01687	0.02585
150	0.02169	0.00830	0.03320	0.00653
180	0.01369	0.02530	0.01483	0.01973
210	0.01871	0.00313	0.00898	0.01129
240	0.00569	0.02816	0.00272	0.03415
270	0.00813	0.04367	0.00735	0.05061
300	0.00569	0.06381	0.00272	0.07089
330	0.00325	0.04109	0.00122	0.04286

Table S4 Transfer integral (hole) for the dimer A, B, A_1, and B_1 (eV) in the full molecular packing (According to the nearest neighbour using B3LYP)

Molecular Pairs	A	B	A_1	B_1
1-2	0.013	0.023	0.016	0.021
1-3	0.006	0.003	0.009	0.083
1-4	4×10^{-4}	0.100	5×10^{-4}	0.100
1-5	0.102	0.137	0.110	0.151
1-6	0.061	0.137	0.075	0.151
1-7	0.020	0.063	0.013	0.076
1-8	0.080	0.196	0.084	0.204
1-9	0.021	1×10^{-4}	0.012	5×10^{-4}
1-10	0.088	0.196	0.104	0.203
1-11	0.065	0.196	0.079	0.203
1-12	0.055	0.063	0.070	0.075
1-13	1×10^{-4}	0.071	0.003	0.097
1-14		0.160		0.175
1-15		0.118		0.113
1-16		1.4×10^{-4}		0.001

Table S5 Transfer integral (hole) for the dimer A, B, A_1, and B_1 (eV) in the full molecular packing (According to the nearest neighbour using GGA)

Molecular Pairs	A	B	A_1	B_1
1-2	2.2×10^{-3}	3.4×10^{-3}	1.8×10^{-3}	3.4×10^{-3}
1-3	1.1×10^{-4}	6×10^{-4}	2.9×10^{-4}	6.5×10^{-5}
1-4	3.6×10^{-5}	1.2×10^{-2}	1.5×10^{-5}	2.3×10^{-2}
1-5	7.8×10^{-3}	2.4×10^{-2}	4.5×10^{-3}	3.6×10^{-2}
1-6	5.5×10^{-3}	2.5×10^{-2}	7.4×10^{-3}	4.1×10^{-2}
1-7	1.2×10^{-3}	3.2×10^{-3}	2.1×10^{-3}	4.1×10^{-3}
1-8	1.7×10^{-3}	2.7×10^{-2}	2.5×10^{-3}	5.3×10^{-2}
1-9	3.2×10^{-3}	3.3×10^{-4}	3.8×10^{-3}	4.2×10^{-4}
1-10	4.4×10^{-3}	2.3×10^{-2}	5.1×10^{-3}	3.8×10^{-2}
1-11	2.1×10^{-3}	3.7×10^{-2}	3.2×10^{-3}	3.7×10^{-2}
1-12	5.7×10^{-3}	7.3×10^{-3}	6.4×10^{-3}	6.2×10^{-3}
1-13	1.3×10^{-5}	8.2×10^{-3}	1.8×10^{-5}	9.3×10^{-3}
1-14		3.5×10^{-2}		4.7×10^{-2}
1-15		2.4×10^{-2}		2.7×10^{-2}
1-16		1.8×10^{-4}		2.9×10^{-4}

Table S6 Transfer integral (electron) A, B, A_1, and B_1 in the full molecular packing (According to the nearest neighbour using B3LYP)

Molecular Pairs	A	B	A_1	B_1
1-2	0.046	0.015	0.045	0.016
1-3	0.009	0.019	0.007	0.204
1-4	6×10^{-4}	0.105	0.001	0.104
1-5	0.164	0.120	0.176	0.128
1-6	0.078	0.120	0.085	0.128
1-7	0.017	0.074	0.040	0.081
1-8	0.033	0.181	0.025	0.187
1-9	0.006	1×10^{-4}	0.029	1×10^{-4}
1-10	0.098	0.181	0.115	0.187
1-11	0.056	0.180	0.074	0.187
1-12	0.066	0.073	0.073	0.081
1-13	0.001	0.075	0.003	0.098
1-14		0.157		0.170
1-15		0.123		0.116
1-16		1×10^{-4}		~0.000

Table S7 Values of planar Angle (°), centre of mass distances [CM(Å)], nearest atoms distances [(NA(Å)], and Transfer Integral [TI(eV)] for the dimers of A

Molecular Pairs	Angle	CM	NA	TI
1-2	41.56	6.87	2.82	2.2×10^{-3}
1-3	56.23	4.60	2.43	1.1×10^{-4}
1-4	27.78	11.83	4.42	3.6×10^{-5}
1-5	38.41	16.07	3.56	7.8×10^{-3}
1-6	49.42	11.82	2.39	5.5×10^{-3}
1-7	21.48	9.95	2.84	1.2×10^{-3}
1-8	59.12	10.43	4.15	1.7×10^{-3}
1-9	18.44	9.76	2.85	3.2×10^{-3}
1-10	2.46	13.42	3.06	4.4×10^{-3}
1-11	16.52	12.39	3.87	2.1×10^{-3}
1-12	51.53	10.81	2.60	5.7×10^{-3}
1-13	26.43	16.75	5.15	1.3×10^{-5}
1-14				
1-15				
1-16				

Table S8 Values of planar Angle (°), centre of mass distances [CM(Å)], nearest atoms distances [(NA(Å)], and Transfer Integral [TI(eV)] for the dimers of B

Molecular Pairs	Angle	CM	NA	TI
1-2	43.23	5.53	2.72	3.4×10^{-3}
1-3	32.85	6.48	2.82	6×10^{-4}
1-4	90.65	5.78	3.88	1.2×10^{-2}
1-5	27.29	11.32	2.75	2.4×10^{-2}
1-6	27.29	11.43	2.61	2.5×10^{-2}
1-7	21.87	11.78	2.18	3.2×10^{-3}
1-8	61.65	13.38	2.92	2.7×10^{-2}
1-9	13.34	16.91	4.21	3.3×10^{-4}
1-10	58.61	13.38	3.42	2.3×10^{-2}
1-11	57.58	13.28	2.92	3.7×10^{-2}
1-12	8.52	11.68	2.28	7.3×10^{-3}
1-13	33.05	16.43	5.36	8.2×10^{-3}
1-14	14.49	17.73	3.95	3.5×10^{-2}
1-15	37.78	15.42	7.23	2.4×10^{-2}
1-16	22.51	14.36	6.29	1.8×10^{-4}

Table S9 Values of planar Angle (°), centre of mass distances [CM(Å)], nearest atoms distances [(NA(Å)], and Transfer Integral [TI(eV)] for the dimers of A_1

Molecular Pairs	Angle	CM	NA	TI
1-2	42.36	6.87	2.82	1.8×10^{-3}
1-3	58.13	4.60	2.83	2.9×10^{-4}
1-4	29.98	12.89	4.42	1.5×10^{-5}
1-5	39.61	16.07	3.76	4.5×10^{-3}
1-6	51.52	11.82	2.39	7.4×10^{-3}
1-7	22.58	9.95	2.84	2.1×10^{-3}
1-8	60.01	11.96	3.85	2.5×10^{-3}
1-9	18.36	9.94	2.85	3.8×10^{-3}
1-10	1.86	14.40	2.76	5.1×10^{-3}
1-11	17.70	12.39	3.87	3.2×10^{-3}
1-12	53.55	11.82	2.40	6.4×10^{-3}
1-13	27.40	17.64	5.15	1.8×10^{-5}
1-14				
1-15				
1-16				

Ramon Valencia-Maturana and Chun-Wei Pao

Table S10 Values of planar Angle (°), centre of mass distances [CM($\mathring{A}$)], nearest atoms distances [(NA($\mathring{A}$)], and Transfer Integral [TI(eV)] for the dimers of B_1

Molecular Pairs	Angle	CM	NA	TI
1-2	43.23	4.58	2.72	3.4×10^{-3}
1-3	32.85	7.22	2.82	6.5×10^{-5}
1-4	90.65	7.68	3.28	$2.3 10^{-2}$
1-5	27.29	10.59	2.75	3.6×10^{-2}
1-6	27.29	10.59	2.61	4.1×10^{-2}
1-7	23.87	10.67	2.18	4.1×10^{-3}
1-8	61.65	12.28	2.92	5.3×10^{-2}
1-9	15.34	15.71	4.21	4.2×10^{-4}
1-10	58.61	12.28	2.92	3.8×10^{-2}
1-11	57.58	12.28	2.92	3.7×10^{-2}
1-12	7.52	10.68	2.18	6.2×10^{-3}
1-13	36.05	15.73	5.36	9.3×10^{-3}
1-14	14.49	18.59	3.95	4.7×10^{-2}
1-15	37.78	16.78	6.20	$2.7 10^{-2}$
1-16	23.51	14.34	6.29	2.9×10^{-4}